

Asymmetry of the photoelectron momentum distribution from molecular ionization in elliptically polarized laser pulses

Ya-Nan Qin,¹ Min Li,^{1,*} Yang Li,¹ Mingrui He,¹ Siqiang Luo,¹ Yali Liu,¹ Yueming Zhou,¹ and Peixiang Lu^{1,2,†}

¹Wuhan National Laboratory for Optoelectronics and School of Physics,
Huazhong University of Science and Technology, Wuhan 430074, China

²Hubei Key Laboratory of Optical Information and Pattern Recognition, Wuhan Institute of Technology, Wuhan 430205, China



(Received 13 November 2018; published 24 January 2019)

We theoretically study the photoelectron momentum distributions (PMDs) of H_2^+ in elliptically polarized laser fields by numerically solving the time-dependent Schrödinger equation. Depending on the internuclear distance of H_2^+ , the PMDs reveal different asymmetries with respect to the major and minor axes of the laser ellipse. At an internuclear distance corresponding to the enhanced ionization region, the asymmetry of the PMDs is opposite to that of the companion atom. We attribute this phenomenon to the effect of the internal scattered electrons, which are mainly released at an earlier ionization moment with respect to the field maximum within each half cycle. We further show that the asymmetry of the PMDs in the elliptical laser fields can be used to identify the instant when the electron wave packet is released from the molecule.

DOI: [10.1103/PhysRevA.99.013431](https://doi.org/10.1103/PhysRevA.99.013431)

I. INTRODUCTION

Atoms or molecules exposed in a strong laser pulse can be tunnel ionized with releasing an electron wave packet. The released electron wave packet can be driven back to the parent ion by the oscillating laser field, which results in many highly nonlinear phenomena, such as high-order above-threshold ionization [1–4], nonsequential double ionization [5,6], and high-order harmonics generation [7–9]. Those processes all depend on the instant when the electron is released within a half cycle of the laser field. For an atom, the bound electron directly tunnels through the suppressed Coulomb barrier. This leads to the expectation that, when the laser field is maximum, the tunneling barrier is the thinnest and the ionization rate of the atom is the highest [10]. In an elliptically polarized laser field, it is expected that the maximal ionization rate corresponds to the instant when the laser field is along the major axis of the laser ellipse and the photoelectron momentum distributions (PMDs) is symmetric with respect to the major and minor axes of the laser ellipse according to the strong-field approximation [11]. In fact, this symmetry is broken by the effect of the Coulomb potential (known as Coulomb asymmetry) [12–14], and the main emission angle in the PMD is shifted to a later ionization moment with respect to the maximum of the laser field.

Compared with the case of an atom, the tunneling ionization of a molecule is more complicated because of the polyatomic Coulomb potential. We take the simplest molecule, i.e., H_2^+ , as an example. As shown in Fig. 1, there might be two barriers formed by the combination of the H_2^+ potential and the external field. When the internuclear distance is

short, the electron tunnels through the outer barrier into the continuum, which is similar to an atom. When the internuclear distance increases to a critical value, an inner barrier between the two nuclei is formed for the molecule. The electron might tunnel through the thin inner barrier from the up-field core. As a result, the ionization rate increases at this critical internuclear distance, which is known as charge-resonance enhanced ionization (EI) [15–23]. The enhancement of the ionization rate and the tunneling site for different internuclear distances have been theoretically predicted and experimentally demonstrated in molecules. Recently, it has been further shown that the shape of the momentum distribution along the laser propagation direction can be used as an indicator of the tunneling site [23].

Moreover, in the EI region of the molecule, it is predicted that there are multiple ionization bursts [18,19,24] within a half cycle of the laser field because of the transient localization of the electrons at one of the nuclei. This indicates a rather complex electron dynamics on the sub-laser-cycle timescale in molecules. Up to now, it is still unclear when the electron wave packets are mainly released from the molecule for different internuclear distances. Furthermore, the spherical symmetry of the Coulomb potential is broken for molecules, which might have a great effect on the electron dynamics of the Coulomb asymmetry in an elliptically polarized laser pulse [25].

In this paper, we study the PMDs of H_2^+ in elliptically polarized laser fields by numerically solving the time-dependent Schrödinger equation (TDSE). The PMD of H_2^+ reveals an asymmetry with respect to the major and minor axes of the laser ellipse, which depends on the internuclear distance. For an internuclear distance corresponding to the EI region, we find that the asymmetry of the PMDs is opposite to that of the companion atom. The asymmetry of the PMDs can not only be used to identify the tunneling site of the molecule, but also

*mli@hust.edu.cn

†lupeixiang@hust.edu.cn

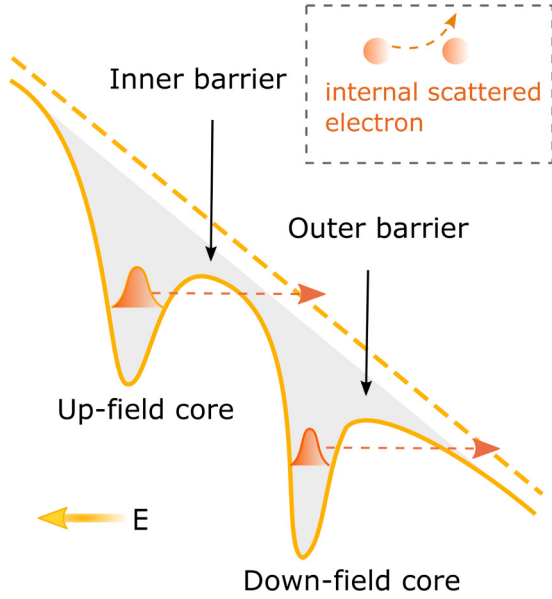


FIG. 1. Sketch of the tunneling ionization of the H_2^+ molecule in a strong electric field. The electron can be released either from the up-field core or from the down-field core depending on the internuclear distance. The inset: the internal scattered electron is referred to as the electron released from the up-field core and then scattered by the down-field core on its subsequent motion.

provide temporal information when the electron tunnels out from the molecule.

II. THEORETICAL METHODS

A. Numerical solutions of the TDSE

We solve the two-dimensional TDSE of fixed-nuclei H_2^+ in an elliptically polarized laser pulse. The TDSE of H_2^+ can be written as [atomic units (a.u.) are used throughout unless specified otherwise]

$$i \frac{\partial}{\partial t} \Psi(\mathbf{r}, t) = H(\mathbf{r}, t) \Psi(\mathbf{r}, t), \quad (1)$$

where $\Psi(\mathbf{r}, t)$ is the electron wave function, $\mathbf{r} = (x, y)$ denotes the electron position, and $H(\mathbf{r}, t)$ is the Hamiltonian. In the length gauge, $H(\mathbf{r}, t)$ is given by

$$H(\mathbf{r}, t) = -\frac{1}{2} \nabla^2 + V(r) + \mathbf{r} \cdot \mathbf{E}(t), \quad (2)$$

where the Coulomb potential is expressed as

$$V(r) = -\frac{1}{\sqrt{(x-R/2)^2 + y^2 + a}} - \frac{1}{\sqrt{(x+R/2)^2 + y^2 + a}}, \quad (3)$$

with R being the internuclear distance. a is the soft-core parameter. For $R = 4$ and 8 a.u., the soft-core parameter is chosen to be 0.72 and 0.723 , corresponding to the ionization potential of H_2^+ of 0.796 and 0.614 a.u., respectively. The elliptically polarized laser field is given by

$$\mathbf{E}(t) = E_0 f(t) \left[\frac{1}{\sqrt{1+\varepsilon^2}} \cos(\omega t) \hat{\mathbf{e}}_x + \frac{\varepsilon}{\sqrt{1+\varepsilon^2}} \sin(\omega t) \hat{\mathbf{e}}_y \right], \quad (4)$$

where E_0 is the electric-field amplitude, ε is the ellipticity, and ω is the angular frequency of the laser pulse. The laser pulse envelope $f(t) = \sin^2(\pi t/T_p)$ is employed with a duration of $T_p = 13T_0$, where T_0 is the period of the 800-nm laser field. To ensure all the ionized components move away from the core, the wave function is further propagated for an additional two optical cycles at the end of the pulse. We use a splitting-operator fast-Fourier transform method to numerically solve the TDSE of the diatomic molecule [26,27]. The ground state of the molecule is obtained by imaginary-time propagation. The whole wave function at any given time τ is split into two parts,

$$\begin{aligned} \Psi(\tau) &= \Psi(\tau)[1 - F_s(R_c)] + \Psi(\tau)[F_s(R_c)] \\ &= \Psi_I(\tau) + \Psi_{II}(\tau). \end{aligned} \quad (5)$$

Here, $F_s(R_c) = 1/(1 + e^{-(r-R_c)/\Delta})$ is an absorbing function that separates the whole space into the inner ($0 \rightarrow R_c$) wave-function $\Psi_I(\tau)$ and outer ($R_c \rightarrow R_{\max}$) wave-function $\Psi_{II}(\tau)$. Ψ_I and Ψ_{II} are propagated under the full Hamiltonian numerically and the Volkov Hamiltonian analytically, respectively. $\Delta = 8$ a.u. represents the width of the crossover region. The photoelectron spectra are obtained from the outer wave function. At each time step, Ψ_{II} is transformed into momentum space,

$$C(\mathbf{p}, \tau) = \int \Psi_{II}(\tau) \frac{e^{-i[\mathbf{p} + \mathbf{A}(\tau)] \cdot \mathbf{r}}}{2\pi} d^2 \mathbf{r}, \quad (6)$$

where $A(\tau)$ is the vector potential of the laser field and Ψ_{II} is propagated to the final time as

$$\begin{aligned} \Psi_{II}(\infty, \tau) &= \int \exp \left\{ -i \int_{\tau}^{\infty} \frac{1}{2} [\mathbf{p} + \mathbf{A}(\tau')]^2 d\tau' \right\} \\ &\quad \times C(\mathbf{p}, \tau) \frac{e^{i\mathbf{p} \cdot \mathbf{r}}}{2\pi} d^2 \mathbf{p} \\ &= \int \bar{C}(\mathbf{p}, \tau) \frac{e^{i\mathbf{p} \cdot \mathbf{r}}}{2\pi} d^2 \mathbf{p}, \end{aligned} \quad (7)$$

so the final momentum distribution is obtained as

$$\frac{dP(\mathbf{p})}{dE d\theta} = \left| \sum_{\tau} \bar{C}(\mathbf{p}, \tau) \right|^2. \quad (8)$$

Here, E is the electron energy associated with \mathbf{p} , and θ is the angle of the emitted electron with respect to the direction of laser polarization.

The PMD of H_2^+ is compared with that of a model atom. The Coulomb potential of the model atom is expressed as $V = -1/\sqrt{x^2 + y^2 + b}$, where $b = 0.325$ corresponds to the ionization potential of 0.614 a.u., which is chosen to match the ionization potential for H_2^+ at $R = 8$ a.u.

In order to gain more details of the electron dynamics, we have traced the time evolution of the electron density along the molecular axis direction, which are obtained by recording electron density at each time step along the x direction [18,19,21,22]. The intensity of the laser field is 1.5×10^{14} W/cm² in the simulation.

B. Classical-trajectory model

The classical-trajectory model is used to analyze the internal scattered electrons (the inset of Fig. 1) at the EI region of H_2^+ , which is similar to the classical rescattering model in Refs. [28,29]. Briefly, the electron is released at one of the nuclei, i.e., $r = (-4, 0)$ a.u. with zero initial longitudinal momentum along the instantaneous laser field direction. A nonzero initial transverse momentum v_\perp is used to compensate the electron motion induced by the rotating electric field. In addition, the ionization time of the electron is restricted within $t_0 \in (0.25, 0.75)T_0$. The electron motion in the laser field is obtained by integrating the classical Newtonian equation without considering the Coulomb effect. Thus, the velocities of the electron along the x and y directions, respectively, can be obtained by

$$\begin{aligned} v_x(t) &= - \int_{t_0}^t E_x(t') dt' = - \frac{E'_0}{\omega} [\sin(\omega t) - \sin(\omega t_0)] + v_{x_0}, \\ v_y(t) &= - \int_{t_0}^t E_y(t') dt' = \varepsilon \frac{E'_0}{\omega} [\cos(\omega t) - \cos(\omega t_0)] + v_{y_0}, \end{aligned} \quad (9)$$

where $E'_0 = E_0/\sqrt{1 + \varepsilon^2}$, $v_{x_0} = v_\perp \sin \phi$, $v_{y_0} = v_\perp \cos \phi$, and $\phi = \arctan(E_y/E_x)$. The electron positions x and y , respectively, can be written as

$$\begin{aligned} x(t) &= - \int_{t_0}^t v_x(t') dt' = \frac{E'_0}{\omega^2} [\cos(\omega t) - \cos(\omega t_0)] \\ &\quad + \omega \sin(\omega t_0)(t - t_0) + v_{x_0}(t - t_0) + x_0, \\ y(t) &= - \int_{t_0}^t v_y(t') dt' = \varepsilon \frac{E'_0}{\omega^2} [\sin(\omega t) - \sin(\omega t_0)] \\ &\quad - \omega \cos(\omega t_0)(t - t_0) + v_{y_0}(t - t_0) + y_0, \end{aligned} \quad (10)$$

where the electron initial positions are $x_0 = -4$ and $y_0 = 0$ a.u. The scattering time t_c is obtained by the conditions that $x(t_c) = 4$ and $y(t_c) = 0$ a.u. The velocities of the electron along the x and y directions, respectively, at the moment of scattering can be given by Eq. (9),

$$\begin{aligned} v_{x_c} &= - \frac{E'_0}{\omega} [\sin(\omega t_c) - \sin(\omega t_0)] + v_{x_0}, \\ v_{y_c} &= \varepsilon \frac{E'_0}{\omega} [\cos(\omega t_c) - \cos(\omega t_0)] + v_{y_0}. \end{aligned} \quad (11)$$

The electron energy E_c and the angle ϕ_c , respectively, with respect to the x direction at the instant of scattering can be calculated by

$$\begin{aligned} E_c &= \frac{1}{2} (v_{x_c}^2 + v_{y_c}^2), \\ \phi_c &= \arccos \frac{v_{x_c}}{\sqrt{v_{x_c}^2 + v_{y_c}^2}}. \end{aligned} \quad (12)$$

With considering the zero scattering angle, the final momentum of the internal scattered electron along the x and y directions, respectively, can be obtained by

$$\begin{aligned} p_x &= \sqrt{2E_c} \cos \phi_c + \frac{E'_0}{\omega} \sin(\omega t_c), \\ p_y &= \sqrt{2E_c} \sin \phi_c - \varepsilon \frac{E'_0}{\omega} \cos(\omega t_c). \end{aligned} \quad (13)$$

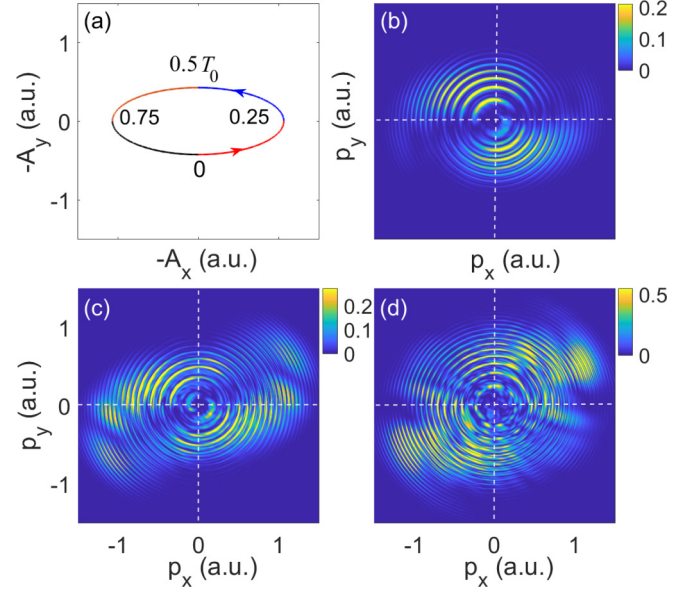


FIG. 2. (a) The field-driven momentum $\mathbf{p} = -\mathbf{A}(t_0)$ for the elliptically polarized laser field. Four segments within each laser cycle of the electric field are shown with different colors, i.e., $0 < t_0 < 0.25T_0$ (red), $0.25T_0 < t_0 < 0.5T_0$ (blue), $0.5T_0 < t_0 < 0.75T_0$ (green), and $0.75T_0 < t_0 < T_0$ (black). (b)–(d) show the PMDs of (b) a model atom, (c) H_2^+ with $R = 4$ a.u., and (d) H_2^+ with $R = 8$ a.u., respectively, in an elliptically polarized laser field ($\varepsilon = 0.4$, $I = 1.5 \times 10^{14}$ W/cm 2 , and $\lambda = 800$ nm).

III. RESULTS AND DISCUSSIONS

We first show the field-driven momentum $\mathbf{p} = -\mathbf{A}(t_0)$ in Fig. 2(a) for the elliptically polarized laser field with an ellipticity of 0.4, where t_0 is the ionization time for the electron. The electric field of the laser pulse consists of four segments per cycle, i.e., $0 < t < 0.25T_0$, $0.25T_0 < t < 0.5T_0$, $0.5T_0 < t < 0.75T_0$, and $0.75T_0 < t < T_0$. The field-driven momenta of those four segments are shown with different colors. Because the ionization time is mapped onto the final momentum, the electrons released at different ionization times are distributed in different regions of the final momentum plane. Figure 2(b) shows the simulated PMD of the model atom in the elliptically polarized laser field ($\varepsilon = 0.4$). One can see many ringlike structures centered by zero momentum, which come from the intercycle interference of the electron wave packets [3,30,31]. As expected, the PMD lacks symmetry with respect to the major and minor axes of the laser ellipse, i.e., most electrons are distributed in the second and fourth quadrants of the momentum plane. This comes from the effect of the Coulomb potential [14]. Compared with Fig. 2(a), one knows that the angular offset for the PMD of the atom tilts to the falling edge of the laser field along the major axis of the laser ellipse, i.e., $0 < t < 0.25T_0$ and $0.5T_0 < t < 0.75T_0$.

We further show the PMDs of H_2^+ for the internuclear distances of $R = 4$ and $R = 8$ a.u. in Figs. 2(c) and 2(d), respectively. The internuclear distance of $R = 8$ a.u. corresponds to the EI region of H_2^+ [23]. Obviously, most electrons are also distributed in the second and fourth quadrants of the momentum plane for $R = 4$ a.u. [Fig. 2(c)]. Compared with the case of the model atom [Fig. 2(b)], the main emission

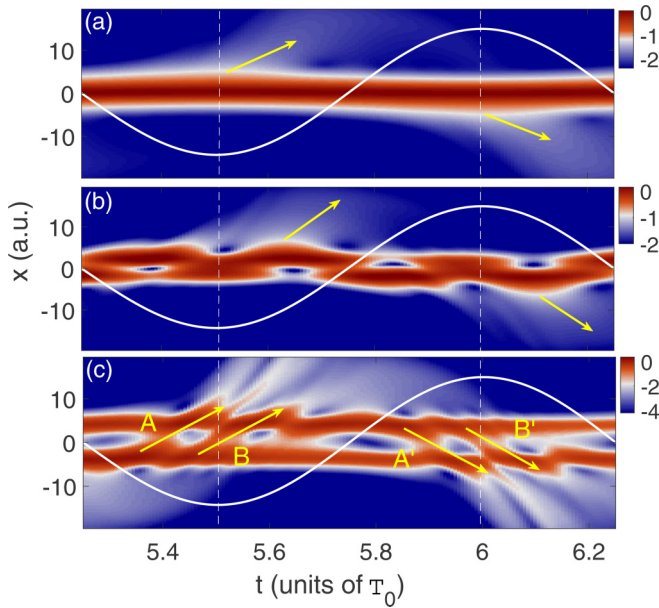


FIG. 3. (a) Electron densities integrated over the y direction for the model atom, (b) H_2^+ at $R = 4$ a.u., and (c) H_2^+ at $R = 8$ a.u. as functions of time and the coordinate x . Note that the color coding is shown on a logarithmic scale. The white solid curves are the laser electric fields along the major axis of the laser ellipse in arbitrary units.

angle is much closer to the major axis of the laser ellipse. When the internuclear distance increases to 8 a.u., as shown in Fig. 2(d), the PMD reveals an opposite asymmetry with that of the atom. Most electrons are distributed in the first and third quadrants of the momentum plane, which correspond to the rising edge of the laser field along the major axis of the laser ellipse, i.e., $0.25T_0 < t < 0.75T_0$ and $0.75T_0 < t < T_0$.

To shed light on the dependence of the asymmetry on the internuclear distance, we have traced the time evolution of the electron density along the molecular axis direction by the TDSE as shown in Fig. 3. For the case of the atom [Fig. 3(a)], the electrons are mainly released near the field maxima of $t = 5.5T_0$ and $t = 6T_0$ as indicated by the arrows. For the case of H_2^+ at $R = 4$ a.u. [Fig. 3(b)], the bound electron density is transiently localized at one of the two protons at $x = \pm 2$ a.u. within a half cycle of the laser field [18,19]. We note that the electrons are mainly released after the field maxima when the bound electron is localized at the down-field core as indicated by the arrows. According to $p = -A(t_0)$, the main emission angle will shift to the major axis compared with that of the atom, which agrees with the PMD in Fig. 2(c). The case is more complex when the internuclear distance increases to 8 a.u. (EI region). As shown in Fig. 3(c), the electron is released in several bunches within a half cycle of the laser field, which is consistent with previous studies [19]. One can clearly see the internal scattered electrons as indicated by the arrows of A, B, A', and B', which is released from the up-field core and then scattered by the down-field core on its subsequent motion [22]. Notably, those internal scattered electrons are mainly released at the rising edge of the laser field along the major axis of the laser ellipse. According to the mapping relation between the ionization time and the final

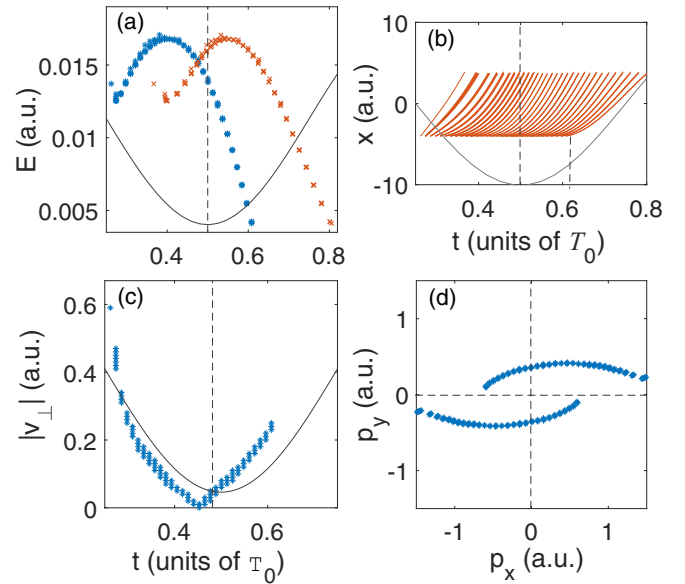


FIG. 4. (a) shows the energy at the instant of scattering with respect to the ionization time (blue asterisk) and the scattering time (orange cross) for the internal scattered electron in H_2^+ with $R = 8$ a.u. calculated by the classical-trajectory model. (b) shows the typical trajectories of the internal scattered electron in the direction of the molecular axis. (c) The absolute value of the initial transverse momentum with respect to the ionization time. In (a)–(c), the gray solid curves are the laser fields along the major axis of the laser ellipse. (d) exhibits the final two-dimensional momenta of the internal scattered electron with assuming zero scattering angle.

momentum, we can infer that those internal scattered electrons are mainly distributed in the first and third quadrants of the final momentum plane. This is consistent with the PMD in Fig. 2(d).

To show why the internal scattered electrons are mainly released at the rising edge of the laser field along the major axis of the laser ellipse at the EI regions, we resort to the classical-trajectory model. Figure 4(a) shows the electron energy at the instant of scattering with respect to the ionization time and the scattering time for the internal scattered electrons of H_2^+ with $R = 4$ a.u. One can see the difference between the scattering time and the ionization time is very small ($\sim 0.2T_0$) for the internal scattered electrons. Figure 4(b) presents the typical trajectories for the internal scattered electron in the direction of the molecular axis. As can be seen, the internal scattered electrons are released before $0.6T_0$, and most of them are released before the field maximum of $0.5T_0$, i.e., the rising edge of the laser field along the major axis of the laser ellipse. The electrons released after the field maximum usually move in a direction away from the parent and neighboring ions at the instant of ionization. They can be driven back to the nuclei after a long traveling time in the laser field. As a result, most of them contribute to the rescattering trajectory instead of the internal scattered trajectory. On the contrary, the electrons released before the field maximum can be directly driven from the parent ion to the neighboring core within a short time interval [$\sim 0.2T_0$ in Fig. 4(a)]. The small difference between the scattering time and the ionization time for the

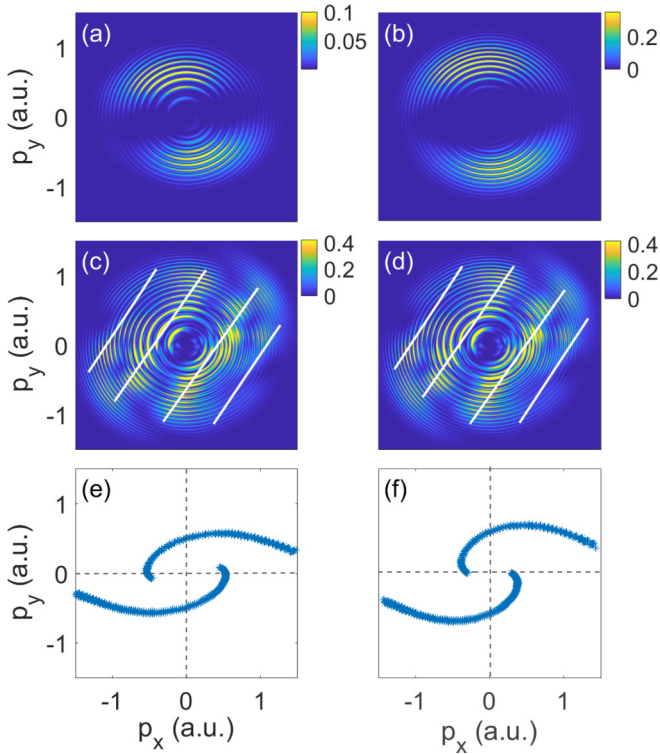


FIG. 5. The PMDs of the model atom [(a) and (b)] and H_2^+ with $R = 8$ a.u. [(c) and (d)] calculated by the TDSE. The white solid lines in (c) and (d) show the maxima of the two-center interference in H_2^+ . (e) and (f) are the final momenta of the internal scattered electron calculated by the classical-trajectory model. The ellipticities of the laser pulses are 0.6 and 0.8 for the left and right columns, respectively.

internal scattered electron mainly has two effects. First, it leads to a small spread of the electron wave packet during the propagation. As a result, the internal scattered electrons have substantial contributions to the PMD. Second, the internal scattered electrons only need a small initial transverse momentum to compensate the transverse motion by the elliptical laser field. We show in Fig. 4(c) the absolute value of the initial transverse momentum for the internal scattered electron with respect to the ionization time. There is a minimum of the absolute value of the initial transverse momentum at $0.45T_0$, which is earlier than the field maximum. According to the tunneling theory [32], the ionization rate from the rising edge of the laser field is larger than that from the falling edge for the internal scattered electrons. Additionally, we present the final momentum of the internal scattered electron with assuming zero scattering angle in Fig. 4(d). One can see that most internal scattered electrons are indeed distributed in the first and third quadrants of the momentum plane, consistent with the TDSE result in Fig. 2(d).

Finally, we show the PMDs of the model atom and H_2^+ with $R = 8$ a.u. calculated by the TDSE in Figs. 5(a)–5(d) in the elliptically polarized laser field with ellipticities of 0.6 and 0.8. For the model atom [Figs. 5(a) and 5(b)], most electrons are distributed in the second and fourth quadrants of the momentum plane for both ellipticities. For H_2^+ in the EI region [Figs. 5(c) and 5(d)], there is an interference

pattern guided by the white solid line, which comes from the two-center interference [33]. Those two-center interference fringes are not perpendicular to the molecular axis due to the effect of the molecular potential on the electron dynamics [33]. Besides those two-center interference fringes, we find that most electrons are distributed in the first and third quadrants of the momentum plane, which differs from the PMDs of the atom [Figs. 5(a) and 5(b)]. In Figs. 5(e) and 5(f), we further show the final momentum of the internal scattered electron calculated by the classical-trajectory model with assuming zero scattering angle. One can see that most electrons are indeed distributed in the first and third quadrants of the momentum plane, which agrees qualitatively with the TDSE results in Figs. 5(c) and 5(d). Thus the internal scattered electrons also have substantial contributions to the PMDs for molecular ionization at the EI region for large ellipticities.

It has been shown recently that the lateral momentum distribution along the laser propagation direction can be dramatically modified by the molecular potential in the EI region [23]. This might also result from the effect of the internal scattered electrons. When the electron wave packet is released from the up-field core and then scattered by the down-field core, the lateral momentum is greatly changed due to the small impact parameter.

From Figs. 2 and 3, we can find that the temporal information of the ionization dynamics of H_2^+ has been imprinted in the asymmetry of the PMDs. Comparing the asymmetry of the PMDs of H_2^+ with that of the atom, one can approximately obtain the instant when the electron wave packet is released from the molecule within a half cycle of the laser field. For the internuclear distance of 4 a.u., the electron wave packet is mainly released from the down-field core after the field maximum. As a result, the main emission angle is shifted to the major axis as compared with the atoms. For the internuclear distance of 8 a.u. (EI region), the electron wave packet is mainly released from the up-field core before the field maximum, leading to the opposite asymmetry of the PMD as compared with the atom. This is consistent with the experimental observation in Ref. [25]. Therefore, the asymmetry of the PMD can be used to identify the instant when the electron is released from the molecule in the elliptically polarized laser pulses.

IV. CONCLUSION

We have studied the PMDs of the H_2^+ molecule and a model atom in elliptically polarized laser fields by numerically solving the TDSE. Depending on the internuclear distance of H_2^+ , the PMDs reveal different asymmetries with respect to the major and minor axes of the laser ellipse. At an internuclear distance corresponding to the EI region, the asymmetry of the PMD is opposite to that of the model atom. We show that the internal scattered electrons have substantial contributions to the PMDs at the EI region of molecules. By tracing the electron density and using a classical-trajectory model, we find that those internal scattered electrons are mainly released at an earlier ionization moment with respect to the field maximum within each half cycle. Thus the asymmetry of the PMD for molecule at the EI region is opposite to that of the model atom. We further show that the asymmetry

of the PMD in the elliptical laser fields has recorded fruitful information about the electron dynamics, which could be used to identify the instant when the electron is released from the molecule within a half cycle of the laser field. Our paper provides a deep understanding on the tunneling ionization of molecules in strong laser fields.

ACKNOWLEDGMENTS

This work was supported by the National Natural Science Foundation of China (Grants No. 11627809, No. 11674116, No. 11722432, and No. 61475055) and the Program for HUST Academic Frontier Youth Team.

-
- [1] P. Agostini, F. Fabre, G. Mainfray, G. Petite, and N. K. Rahman, *Phys. Rev. Lett.* **42**, 1127 (1979).
- [2] W. Becker, F. Grabon, R. Kopold, D. B. Milošević, G. G. Paulus, and H. Walther, *Adv. At. Mol. Opt. Phys.* **48**, 35 (2002).
- [3] M. Li, J.-W. Geng, H. Liu, Y. Deng, C. Wu, L.-Y. Peng, Q. Gong, and Y. Liu, *Phys. Rev. Lett.* **112**, 113002 (2014).
- [4] D. B. Milošević, G. G. Paulus, and W. Becker, *Opt. Express* **11**, 1418 (2003).
- [5] W. Becker, X. Liu, P. J. Ho, and J. H. Eberly, *Rev. Mod. Phys.* **84**, 1011 (2012).
- [6] D. N. Fittinghoff, P. R. Bolton, B. Chang, and K. C. Kulander, *Phys. Rev. Lett.* **69**, 2642 (1992); X. Ma, Y. Zhou, N. Li, M. Li, and P. Lu, *Opt. Laser Technol.* **108**, 235 (2018).
- [7] Y. Mairesse, A. de Bohan, L. J. Frasinski, H. Merdji, L. C. Dinu, P. Monchicourt, P. Breger, M. Kovačev, R. Taïeb, B. Carré, H. G. Muller, P. Agostini, and P. Salières, *Science* **302**, 1540 (2003).
- [8] F. Krausz and M. Ivanov, *Rev. Mod. Phys.* **81**, 163 (2009).
- [9] L. He, P. Lan, A.-T. Le, B. N. Wang, B. C. Wang, X. Zhu, P. Lu, and C. D. Lin, *Phys. Rev. Lett.* **121**, 163201 (2018); H. Yuan, L. He, B. Wang, X. Zhu, P. Lan, and P. Lu, *Opt. Lett.* **43**, 931 (2018).
- [10] M. Uiberacker, T. Uphues, M. Schultze, A. J. Verhoef, V. Yakovlev, M. F. Kling, J. Rauschenberger, N. M. Kabachnik, H. Schröder, M. Lezius, K. L. Kompa, H.-G. Muller, M. J. J. Vrakking, S. Hendel, U. Kleineberg, U. Heinzmann, M. Drescher, and F. Krausz, *Nature (London)* **446**, 627 (2007).
- [11] L. V. Keldysh, *Sov. Phys. JETP* **20**, 1307 (1965).
- [12] M. Bashkansky, P. H. Bucksbaum, and D. W. Schumacher, *Phys. Rev. Lett.* **60**, 2458 (1988).
- [13] S. P. Goreslavski, G. G. Paulus, S. V. Popruzhenko, and N. I. Shvetsov-Shilovski, *Phys. Rev. Lett.* **93**, 233002 (2004).
- [14] M. Li, Y. Liu, H. Liu, Q. Ning, L. Fu, J. Liu, Y. Deng, C. Wu, L.-Y. Peng, and Q. Gong, *Phys. Rev. Lett.* **111**, 023006 (2013).
- [15] T. Zuo and A. D. Bandrauk, *Phys. Rev. A* **52**, 2511(R) (1995).
- [16] T. Seideman, M. Y. Ivanov, and P. B. Corkum, *Phys. Rev. Lett.* **75**, 2819 (1995).
- [17] E. Constant, H. Stapelfeldt, and P. B. Corkum, *Phys. Rev. Lett.* **76**, 4140 (1996).
- [18] N. Takemoto and A. Becker, *Phys. Rev. Lett.* **105**, 203004 (2010).
- [19] N. Takemoto and A. Becker, *Phys. Rev. A* **84**, 023401 (2011).
- [20] J. Wu, M. Meckel, L. Ph. H. Schmidt, M. Kunitski, S. Voss, H. Sann, H. Kim, T. Jahnke, A. Czasch, and R. Dörner, *Nat. Commun.* **3**, 1113 (2012).
- [21] C. Huang, P. Lan, Y. Zhou, Q. Zhang, K. Liu, and P. Lu, *Phys. Rev. A* **90**, 043420 (2014).
- [22] Y. Li, Y. Zhou, M. He, M. Li, P. Lan, and P. Lu, *Phys. Rev. A* **94**, 013422 (2016).
- [23] K. Liu and I. Barth, *Phys. Rev. Lett.* **119**, 243204 (2017).
- [24] K. Codling, L. J. Frasinski, and P. A. Hatherly, *J. Phys. B: At., Mol. Opt. Phys.* **22**, L321 (1989).
- [25] J. Wu, M. Meckel, S. Voss, H. Sann, M. Kunitski, L. Ph. H. Schmidt, A. Czasch, H. Kim, T. Jahnke, and R. Dörner, *Phys. Rev. Lett.* **108**, 043002 (2012).
- [26] X. M. Tong, K. Hino, and N. Toshima, *Phys. Rev. A* **74**, 031405(R) (2006).
- [27] J. Tan, Y. Zhou, M. Li, M. He, Y. Liu, and P. Lu, *Opt. Express* **26**, 20063 (2018); J. Tan, Y. Zhou, M. He, Y. Chen, Q. Ke, J. Liang, X. Zhu, M. Li, and P. Lu, *Phys. Rev. Lett.* **121**, 253203 (2018); X. Zhang, X. Zhu, D. Wang, L. Li, X. Liu, Q. Liao, P. Lan, and P. Lu, *Phys. Rev. A* **99**, 013414 (2019).
- [28] X. Zhang, L. Li, X. Zhu, X. Liu, Q. Zhang, P. Lan, and P. Lu, *Phys. Rev. A* **94**, 053408 (2016).
- [29] M. Li, W. C. Jiang, H. Xie, S. Luo, Y. Zhou, and P. Lu, *Phys. Rev. A* **97**, 023415 (2018).
- [30] M. Murakami and S.-I. Chu, *Phys. Rev. A* **93**, 023425 (2016).
- [31] H. Xie, M. Li, S. Luo, Y. Li, Y. Zhou, W. Cao, and P. Lu, *Phys. Rev. A* **96**, 063421 (2017).
- [32] N. B. Delone and V. P. Krainov, *J. Opt. Soc. Am. B* **8**, 1207 (1991).
- [33] W. Yang, Z. Sheng, X. Feng, M. Wu, Z. Chen, and X. Song, *Opt. Express* **22**, 002519 (2014).